

# An observational case study of mesoscale atmospheric circulations induced by soil moisture.

Christopher M. Taylor<sup>1</sup>, Douglas J. Parker<sup>2</sup>, Phil P. Harris<sup>1</sup>

1. Centre for Ecology and Hydrology, Wallingford, Oxfordshire, OX10 8BB, U.K.  
2. University of Leeds, Leeds, U.K.

An edited version of this paper was published by AGU. Copyright 2007 American Geophysical Union.

Taylor, C. M., D. J. Parker, and P. P. Harris (2007), An observational case study of mesoscale atmospheric circulations induced by soil moisture, *Geophys. Res. Lett.*, 34, L15801, doi:10.1029/2007GL030572.

## ***Abstract***

Numerical and theoretical studies have shown that mesoscale gradients in land surface properties can induce circulations in the atmosphere. This study provides the first well-resolved observations of such flows induced by soil moisture from recent rainfall, and is based on aircraft data in the Sahel. Satellite imagery was used to identify fine scale soil moisture features within a wet zone spanning 160 km. Above the wet soil, the planetary boundary layer was up to 3 K cooler, 3 gkg<sup>-1</sup> moister and extended to only half the depth of nearby drier areas. Mesoscale perturbations to the background flow were found, consistent with low level divergence over wet soil and convergence in drier areas. The soil moisture and atmospheric wind patterns were statistically coherent on wavelengths down to 20km. These results suggest that mesoscale convergence lines forced by soil moisture may play a significant role in the meteorology of the Sahel.

## ***1. Introduction***

The impact on the planetary boundary layer (PBL) of mesoscale variations in surface properties such as vegetation cover and soil moisture has been a subject of research for over two decades (e.g. *Ookouchi et al.*, 1984, *Mahfouf et al.*, 1987). There have been many modelling studies which have shown that surface heterogeneity can generate sea-breeze-like circulations (see a summary by *Segal and Arritt*, 1992 of such Non-classical Mesoscale Circulations, or NCMCs). Numerical and theoretical studies indicate a strong sensitivity of the mesoscale flow to the background wind conditions, as well as the amplitude and the length scale of the surface heat flux contrast. The role of the circulations in initiating moist convection has also been studied (e.g. *Chen and Avissar*, 1994, *Weaver*, 2004, *Cheng and Cotton*, 2004)

There has been relatively little observational evidence to support the modelling studies, leading some (e.g. *Shaw and Doran*, 2001) to question the importance of surface-forced circulations in overall land-atmosphere interaction. Examples of observed

5 circulations include the impact of irrigated areas (*Mahrt et al.*, 1994) and snow cover (*Segal et al.*, 1991, *Taylor et al.*, 1998). There has been no compelling observational evidence of flows induced by soil moisture from antecedent rainfall, yet the dynamical nature of this forcing would represent an important “internal” climatic feedback on time

10 The Sahel is a region of the world where intense convective rain events generate marked spatial and temporal variability in near surface soil moisture. The surface energy balance here is influenced strongly by surface moisture via high rates of evaporation directly from the soil in the first few days after rain. Observations from the JET2000 aircraft campaign indicated how soil moisture patterns affected temperature and humidity in the PBL (*Taylor et al.*, 2003). The JET2000 flight had not targeted soil moisture variability explicitly, and it was not possible to isolate any dynamical response to the soil moisture in that case. During the Special Observing Period of the African Monsoon Multidisciplinary Analyses study (AMMA; *Redelsperger et al.*, 2006), soil moisture features were deliberately targeted by the BAe 146 operated by the U.K. Facility for Airborne Atmospheric Measurements. One of the aims of these flights was to establish whether the soil moisture (and associated heating) gradients were strong enough to induce atmospheric circulations in a given background flow. This study presents the first results from that campaign, and these strongly support the hypothesis.

## 20 ***2. Data and Conditions on 1 August 2006***

25 During the observational campaign, land surface temperature (LST) data produced operationally by the LandSAF from SEVIRI observations onboard the MSG satellite (*Wan and Dozier*, 1996) were used to locate strong gradients in soil moisture. The use of thermal satellite data to infer soil moisture status is well-established (e.g. *Wetzel et al.*, 1984) and was found to be effective in locating recent storms in the JET2000 experiment (*Taylor et al.*, 2003). Additional cloud screening was applied to the LandSAF data based on the time evolution of the thermal and visible channels, following *Taylor et al.* (2003). This process reduced greatly the contamination of the land surface signal by cloudy and dusty pixels which were not flagged by the Eumetsat operational screen. For each pixel the impact of transient wet soil conditions on LST was separated from more permanent factors such as land cover by computing the LST anomaly (LSTA) from the 21-day running mean for the corresponding time of day. Recently wetted pixels are typically cooler than the longer-term mean. Finally, LSTA data from every 15 minute slot between 0700 and 1700 (local time) were averaged to produce a daily LSTA summary. The data were invaluable for flight planning, enabling paths to be designed over fresh soil moisture features once the sun had come up, in the absence of clouds. The data provided a qualitative measure of soil moisture, and in particular, distinguished between dry and recently wetted surfaces.

40 This case study concerns a flight on 1 August 2006 undertaken to the north-west of Niamey (13.5 °N, 2.3 °E) in Niger and into Mali (see Figure 1), covering a straight track of 470 km. Whilst the region directly to the north of Niamey was undergoing a dry spell, there had been a series of storms in the preceding days north of around 15 °N, including a major storm which initiated during the previous afternoon close to 16 °N, 1 °E. This major convective system subsequently travelled across Mali, leaving a swath of wet soil several hundred kilometres across and over 1000 km long. Within this large-

scale storm path, many fine scale cool (wet) surface features are evident in Figure 1b, consistent with the convection which was tracked from thermal imagery during the storm.

5 The aim of the flight was to sample the PBL above the contrasting soil moisture conditions near the north-eastern end of the track of this storm. The flight took place during the early afternoon, when any daytime dynamical response to the surface would be maximised, while the bulk properties of the boundary layer were varying relatively slowly with time. The flight consisted of a leg at minimum safe altitude (170 m above ground level, 13:06 to 14:12 UTC) headed approximately north-west across the soil moisture pattern into Mali from Niger. This was followed by a return leg at an altitude of 10 7000 m (14:35 to 15:29 UTC) from which dropsondes were launched. The first leg provided high spatial resolution temperature, humidity and wind data whilst the second gave an indication of the vertical structure of the atmosphere at reduced horizontal resolution. The terrain on the flight track was rather flat. North of 15.0 °N, topographic height varied by up to 30m around a mean of 300m, whilst further south, the aircraft 15 crossed larger valleys of up to 60 m depth. The vegetation was generally very sparse, with a seasonal herbaceous layer just starting to emerge between woody coverage of a few percent.

The synoptic conditions during the flight were dominated by an African Easterly Wave. A trough had passed over the region the previous day, and the low level flow on 20 August was south-westerly, as depicted by the European Centre for Medium Range Weather Forecasts (ECMWF) analysis at 925 hPa (Figure 1a). During the low level flight, the track was predominantly cloud-free north of 15.0 °N. The PBL became markedly dustier north of 16.7 °N, and this may have affected the quality of the LSTA and onboard radiometer data in the north of the transect.

25 Data from the aircraft used here included temperature, humidity and 3-dimensional wind observations, all recorded at 32 Hz (<http://www.faam.ac.uk/>). In addition to calculating mean dynamic and thermodynamic variables from these sensors, an estimate of sensible heat flux at the level of the flight was computed based on the covariance of the temperature and the vertical velocity about 30 second running means 30 (approximately 3 km). A Heimann radiometer was used to identify variations in land surface temperature directly beneath the aircraft. Finally, an Airborne Vertical Atmospheric Profiling System comprising Vaisala RD93 dropsondes was deployed.

### ***3. Variability at the Surface and in the Planetary Boundary Layer***

35 A qualitative assessment of the rainfall history along the flight track was developed based on LSTA data (spatial pattern) and cold cloud imagery (timing of the storms that wetted the surface). The 2-dimensional structure of the wet features on or near the track (Figure 1b) could be associated with convective-scale structure in the earlier evolution of the cold cloud. For clarity, we defined 6 wet surface patches based on gradients in LSTA along the flight track (Figure 2). Soil moisture from the storm on 31 40 July produced strong surface cooling beneath the flight track between 16.1 and 16.45 °N (patch 5), and again around 16.6 °N (patch 6). Distinct soil moisture features remained from storms on 30 July between 15.5 and 16.1 °N (patches 2, 3 and 4), although these zones were far from uniformly wet. For example, patch 4 (due to an event on 30 July) was as marked in terms of LSTA as that produced by the storm on the previous afternoon 45 (negative anomalies exceeding 7 °C), whilst patches 2 and 3 were relatively dry. A weak

LSTA pattern was also identified further south (patch 1) associated with a storm 4 days earlier. Finally, north of patch 6, rain events on 30 July had produced widespread negative LSTAs. By the time of the flight (2 days later), these features were rather weak and not so well-defined in space.

5 Figure 2 presents a series of datasets plotted as a function of latitude along the 470 km track. Figure 2a demonstrates the impact of near surface moisture (as detected through LSTA) on the surface energy balance. Variations in surface temperature recorded by the aircraft radiometer were generally well correlated with LSTA. Similarly, a positive correlation was evident between turbulent heat flux and LSTA. These relationships were  
10 weaker in the drier zones at either end of the transect, with the clearest example of cooler surface temperatures and reduced heat fluxes (in the absence of near surface moisture) being between 14.6 and 14.9 °N. This was a relatively well-vegetated valley where evaporation could be maintained in spite of a lack of recent rain via transpiration from the root zone. Furthermore, downwelling surface radiation was reduced in this region due to  
15 cloud.

The spatial pattern of heating along the track produced a clear response to surface wetness in the PBL potential temperature (Figure 2b). Compared to the large scale temperature trend (illustrated by the midday ECMWF analysis at 1° resolution), the PBL was observed to be up to 3K cooler in the wet zone compared to adjacent drier zones.  
20 This atmospheric response was qualitatively similar to previous observations (*Taylor et al.*, 2003), but the amplitude of temperature variations was 2K stronger in this case. The surface wetness also induced substantial variations in PBL humidity, notably in the positive local anomalies of around 3-4 gkg<sup>-1</sup> where the previous day's storm occurred.

In Figure 2c, the impact of surface-induced PBL gradients on the wind is shown.  
25 There was a strong positive correlation between the along-track gradient in virtual potential temperature and the wind component in that direction. As discussed above, these PBL gradients were linked to gradients in LSTA. Thus, in the storm-affected central zone, local minima in (roughly) south-easterly wind speed occurred at 15.48, 15.75, 15.91 and 16.50 °N, to the south-east of patches 2, 3, 4 and 6, with wind anomalies of  
30 around 1-2 ms<sup>-1</sup>. Conversely, there was a tendency for local maxima in along-track wind to occur close to where the aircraft flew from a wet to a dry surface. Thus zones of horizontal divergence were located approximately over the wet patches, consistent with earlier studies (e.g. *Ookouchi et al.*, 1984). A further divergent flow was identified over the cool, well-vegetated patch (14.6-14.9 °N) within the dry soil region. Taking values for  
35 winds over the dry slot around 16.5 °N, along-track convergence reached values of 10<sup>-4</sup> s<sup>-1</sup>. Assuming a vertical length scale for such a circulation of 1.5 km implies a peak vertical velocity in the middle of the PBL of the order of 7.5 cm s<sup>-1</sup>, the same order of magnitude as has been simulated numerically by various authors.

Given the fine spatial resolution of the flow (features on scales ~20 km), the  
40 dropsondes (spaced typically 75 km apart) could not provide a comprehensive cross-section of the mesoscale flows. However, they illustrated the vertical structure of the surface-induced PBL anomalies at a number of locations on the flight track. In Figure 3, the profiles at 15.0 and 16.0 °N are contrasted. Above patch 4 at 16.0 °N, the well-mixed layer extended to 910 hPa, compared to 820 hPa over dry soil at 15.0 °N. The mixed layer  
45 values of potential temperature and specific humidity were consistent with those measured on the low level leg at 960 hPa (Figure 2b). The dropsonde wind data showed

the south-westerly monsoon flow at 15 °N (and also 14.6 °N, not shown). At 16.0N on the other hand, the winds had a stronger westerly component and notably weaker southerlies in the PBL. Above the PBL there was a weak southerly jet at 850 hPa. The dropsonde winds were consistent with the onboard low level data and indicate divergence up to 875 hPa over the major storm track.

#### 4. Spatial scale of dynamical response

Having aircraft measurements at high resolution allowed us to quantify the dependence of this response on spatial scale, using spectral analysis. Onboard estimates of surface temperature from the Heimann radiometer were used with in-situ measurements of thermodynamic data and along-track winds, all averaged to 100 m along the track and detrended. The spectral analysis outlined by *Matthews and Madden (2000)* has then been applied in terms of spatial transforms, in order to quantify the spectral coherency as a function of spatial scale (or wavenumber). The coherency between two Fourier transforms is usually described as a spectral version of the correlation function, and is based on the product of one spectrum with the complex conjugate of the other. Smoothing of this product is required, here using a running mean, in order to infer significance over a range of wavenumbers, with this range corresponding to the bandwidth. The result is normalised by the smoothed amplitudes of the original spectra to deduce the coherency, which takes values in the range from zero to one. If a consistent relationship between the spectra exists over a range of wavenumbers, then the coherency will be high.

Figure 4 shows a plot of coherency squared for the surface temperature with, respectively, along-track wind component and virtual potential temperature. The 95% confidence level is plotted following *Julian (1975)*. For low wavenumbers, Figure 4 confirms the conclusions which can be inferred by eye in Figure 2; that there is strong coherency between surface temperature and both wind and temperature in the PBL. Furthermore, from Figure 4 we can state that in this case the coupling between winds and surface temperatures was significant on wavelengths down to 20 km (wavenumber 0.05 c/km), equivalent to adjacent wet and dry patches of 10 km scale. Coupling of surface and PBL temperatures was significant on smaller scales, arguably down to 5 km wavelength. The scale of mixing by large boundary layer eddies is on the scale of the PBL depth – around 1km – and therefore the loss of coherency between atmospheric and surface temperature details below 5 km is not unexpected. Note that the coherency between the *across-track* component of the wind and the surface temperature is not statistically significant at the 95% level in these data. These results appear to be robust, in that they are not sensitive to reasonable changes in the spectral bandwidth.

The phase function (inset, Figure 4) confirmed that the convergence of warm air occurred over the warmer surfaces (phase of around 90°) at wavelengths down to 40 km. However, at shorter surface length scales, the phase increased, so that at a wavelength of 20 km, the wind and surface temperature patterns were almost in anti-phase (150 degrees). This implies that convergence was maximised to the south-east of a given warm surface anomaly; a feature which may be inferred by eye from Figure 2c. The gain function – the amplitude of the atmospheric response to a given amplitude of surface temperature – showed that the gain of the convergent response along the track was not

significantly sensitive to length scale, and, consistently, that gain in along-track winds increased with horizontal scale (inset Figure 4), having values consistent with those described in section 3.

## 5. Discussion

5 This study has shown for the first time from observations that rainfall can generate sufficient spatial variability in soil moisture and heat flux to affect the low level wind field on scales of 10 km upwards. The satellite data in Figure 1a indicate that the soil beneath the 31 July storm path was rather wetter further downstream, where the system had matured into a major mesoscale convective system, than in the location of the flight. This suggests that PBL temperature gradients and associated convergence features may have been even stronger to the south-west than were observed here. On 1 August 2006, there were 3 major soil moisture features from storm tracks across the Sahel (Figure 1a). The occurrence of such soil moisture forcing during the wet season should therefore perhaps be regarded as the norm, and the occurrence of surface-induced mesoscale circulations as daily events. The Sahel provides very favourable conditions for moisture-induced circulations to develop. In regions with denser vegetation, where surface fluxes are influenced more by root zone soil moisture accumulated over many rain events, spatial variability will tend to be weaker, and circulations less likely.

20 The strength of the response and the lack of distortion by the large-scale flow in this case were presumably linked with the approximate alignment of the background wind with the principal wet feature, both approximately south-westerly, and the choice of a flight path roughly perpendicular to this axis. Analysis of additional flights during the AMMA campaign under contrasting atmospheric conditions will shed further light on this issue. They may also provide evidence for nocturnal amplification of surface-induced circulations, as proposed by *Parker et al.* (2005).

25 Work is needed to quantify the surface flux patterns associated with soil moisture variability, based on land surface models forced by the best available meteorological forcing (notably rainfall). This will provide an opportunity to test both theoretical and numerical models of NCMCs. Finally, it is important to use observations from AMMA to examine whether these circulations play a direct role in triggering moist convection. The recent observational study by *Taylor and Ellis* (2006) identified that afternoon convection in this region is modulated by soil moisture, with strong suppression of initiation over wet soils. This modulation is consistent with NCMC forcing.

## Acknowledgements

35 We would like to warmly thank all those involved in the Niger deployment of the FAAM aircraft, the staff at LandSAF for providing land surface temperature data, and Adrian Matthews for assistance with flight planning and statistical analysis. Based on a French initiative, AMMA was built by an international scientific group and is currently funded by a large number of agencies, especially from France, the UK, the US and Africa. This study was funded jointly by the European Community's Sixth Framework Research Programme and the UK NERC project NE/B505597/1.

## References

- Chen, F., and R. Avissar (1994), Impact of land-surface moisture variability on local shallow convective cumulus and precipitation in large-scale models, *J. Appl. Meteorol.*, *33*, 1382-1401.
- Cheng, W. Y. Y., and W. R. Cotton (2004), Sensitivity of a cloud-resolving simulation of the genesis of a mesoscale convective system to horizontal heterogeneities in soil moisture initialization, *J. Hydromet.*, *5*, 934-958.
- Julian, P. R. (1975), Comments on the determination of significance levels of the coherency statistic, *J. Atmos. Sci.*, *32*, 836-837.
- Mahfouf, J. F., E. Richard, and P. Mascart (1987), The influence of soil and vegetation on the development of mesoscale circulations, *J. Clim. Appl. Meteorol.*, *26*, 1483-1495.
- Mahrt, L., J. L. Sun, D. Vickers, J. I. MacPherson, J. R. Pederson, and R. L. Desjardins (1994), Observations of fluxes and inland breezes over a heterogeneous surface, *J. Atmos. Sci.*, *51*, 2484-2499.
- Matthews, A. J., and R. A. Madden (2000), Observed propagation and structure of the 33-h atmospheric Kelvin wave, *J. Atmos. Sci.*, *57*, 3488-3497.
- Njoku, E. G. (2004), AMSR-E/Aqua daily L3 surface soil moisture, interpretive parms, & QC EASE-Grids, edited, National Snow and Ice Data Center, Boulder, CO, USA.
- Ookouchi, Y., M. Segal, R. C. Kessler, and R. A. Pielke (1984), Evaluation of soil moisture effects on the generation and modification of mesoscale circulations, *Mon. Weather Rev.*, *112*, 2281-2292.
- Parker, D. J., R. R. Burton, A. Diongue-Niang, R. J. Ellis, M. Felton, C. M. Taylor, C. D. Thorncroft, P. Bessemoulin, and A. M. Tompkins (2005), The diurnal cycle of the West African monsoon circulation, *Quart J Roy Meteorol Soc.*, *131*, 2839-2860.
- Redelsperger, J. L., C. D. Thorncroft, A. Diedhiou, T. Lebel, D. J. Parker, and J. Polcher (2006), African Monsoon Multidisciplinary Analysis - An international research project and field campaign, *Bull. Am. Meteorol. Soc.*, *87*, 1739-+.
- Segal, M., and R. W. Arritt (1992), Nonclassical mesoscale circulations caused by surface sensible heat-flux gradients, *Bull. Am. Meteorol. Soc.*, *73*, 1593-1604.
- Segal, M., J. H. Cramer, R. A. Pielke, J. R. Garratt, and P. Hildebrand (1991), Observational evaluation of the snow breeze, *Mon. Weather Rev.*, *119*, 412-424.
- Shaw, W. J., and J. C. Doran (2001), Observations of systematic boundary layer divergence patterns and their relationship to land use and topography, *J. Climate* *14*, 1753-1764.
- Taylor, C. M., and R. J. Ellis (2006), Satellite detection of soil moisture impacts on convection at the mesoscale, *Geophys. Res. Lett.*, *33*, L03404.
- Taylor, C. M., R. J. Ellis, D. J. Parker, R. R. Burton, and C. D. Thorncroft (2003), Linking boundary-layer variability with convection: A case- study from JET2000, *Q. J. R. Meteorol. Soc.*, *129*, 2233-2253.
- Taylor, C. M., R. J. Harding, R. A. Pielke, P. L. Vidale, R. L. Walko, and J. W. Pomeroy (1998), Snow breezes in the boreal forest, *J. Geophys. Res. - Atmospheres*, *103*, 23087-23101.
- Wan, Z., and J. Dozier (1996), A generalised split-window algorithm for retrieving land-surface temperature from space, *IEEE Transactions on Geoscience and Remote Sensing*, *34*, 892-905.

Weaver, C. P. (2004), Coupling between large-scale atmospheric processes and mesoscale land-atmosphere interactions in the US Southern Great Plains during summer. Part I: Case studies, *J. Hydromet.*, 5, 1223-1246.

Wetzel, P. J., D. Atlas, and R. H. Woodward (1984), Determining Soil-Moisture from Geosynchronous Satellite Infrared Data - a Feasibility Study, *J. Clim. Appl. Meteorol.*, 23, 375-391.

## Figures

Figure 1 The path of the aircraft on 1 August 2006 (solid line). (a) Surface soil moisture [m<sup>3</sup>/m<sup>3</sup>] across West Africa produced from AMSR-E data by NASA (*Njoku, 2004*). When data are available from two overpasses on 1 August, the mean value is shown. The edges of the early afternoon swaths are marked with dashed lines, and overpass times (UTC) are marked at the top. Note that the storm which initiated close to the flight track was not detected west of 6 °W as it had not reached this region by the overpass time (02:30 1 August). Also shown are the wind vectors at 925 hPa from the midday ECMWF operational analysis. The dashed rectangle shows the domain of Figure 1b. (b) Daily land surface temperature anomaly summary in the region of the flight (shading). The dashed contours at -60, -70 and -80 °C indicate the minimum temperatures measured by MSG during the storm of the previous day (1400 – 2400 UTC). The locations of dropsonde descents are shown by triangles.

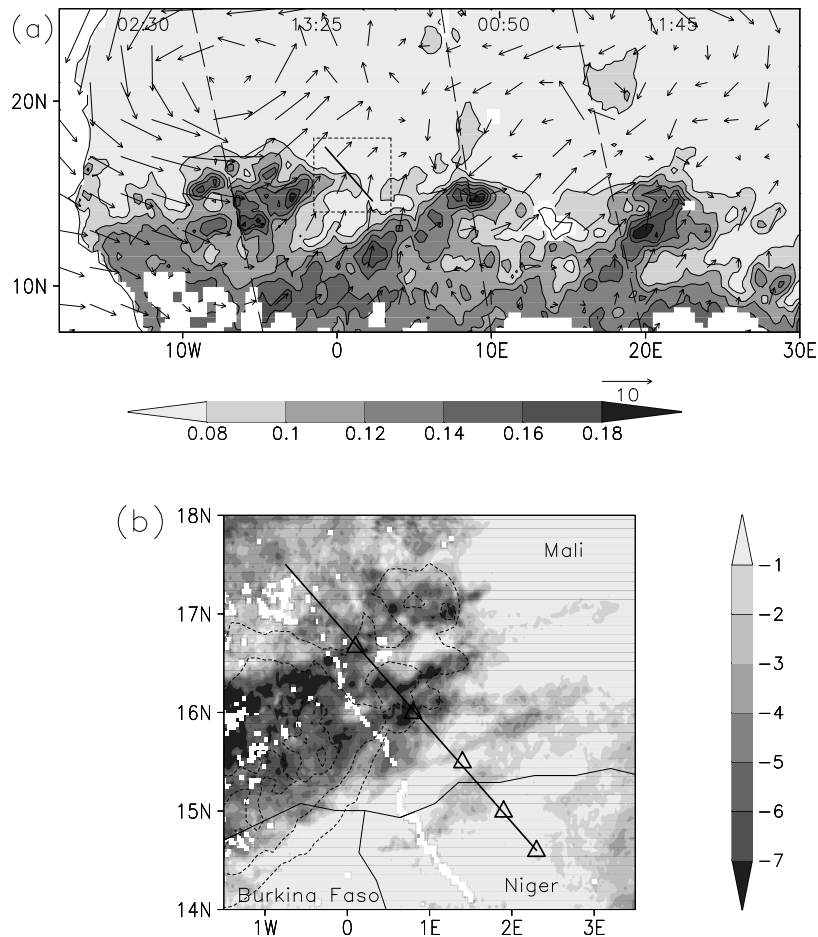


Figure 2. Aircraft data from the low level transect. Satellite-derived land surface temperature anomaly (LSTA; grey shading) is shown in Figures 2a and 2b. (a): Surface temperature from the onboard radiometer (solid line) and turbulent heat flux (squares). (b): Potential temperature (solid) and humidity mixing ratio (squares), and potential temperature at 925hPa in the midday ECMWF analysis (dashed). (c): Along-track component of the wind (solid) and gradient in virtual potential temperature (dashed). The solid black rectangles denote wet patches identified using gradients of LSTA.

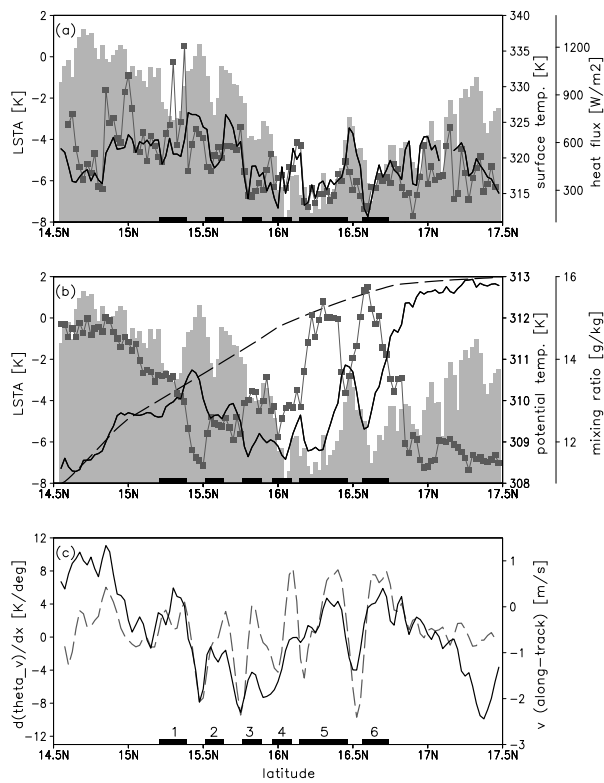


Figure 3. Vertical profiles from dropsondes at 15 and 16 °N.

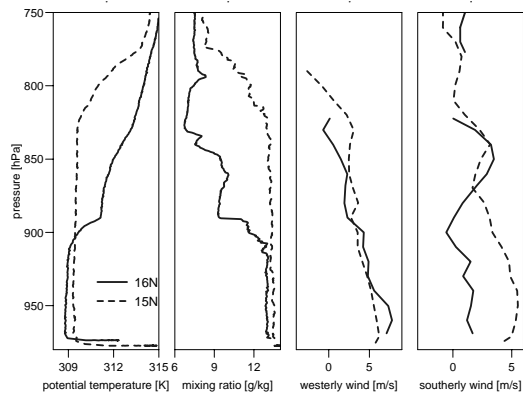


Figure 4: Coherency squared for along-track wind component with surface temperature (solid line) and virtual potential temperature with surface temperature (dashed), as a function of wavenumber in cycles/km. Inset is the phase functions for these pairs of measurements, and the gain function for along-track wind with surface temperature (dotted).

